PIER C

(Received 9 April 2024, Accepted 15 July 2024, Scheduled 15 August 2024)

Performance Analysis of Stator Structure in Divided Teeth Outer Rotor Embedded Permanent Magnet Synchronous Motor: Salient Pole Stator vs Segmented Stator

Hairul F. Hairulnizam[1,*], Norhisam Misron[1,2,3,*], Nur A. Ibrahim[1], Ezwan Muhammad[1], and Chockalingam A. Vaithilingam[4,5]

[1] *Faculty of Engineering, Universiti Putra Malaysia, Serdang 43400, Selangor, Malaysia*
[2] *Institute of Nanoscience and Nanotechnology, Universiti Putra Malaysia, Serdang 43400, Selangor, Malaysia*
[3] *Institute of Plantation Studies, Universiti Putra Malaysia, Serdang 43400, Selangor, Malaysia*
[4] *Clean Technology Impact Lab, Taylor's University, Subang Jaya 47500, Selangor, Malaysia*
[5] *Vel tech Rangarajan Dr. Sanguthala R and D Institute of Science and Technology, Chennai 600092, Tamilnadu, India*

ABSTRACT: To improve torque characteristics, this study proposes an upgrade over the standard salient pole stator in a Permanent Magnet Synchronous Motor (PMSM) using a segmented stator. The rotor is externally oriented and has a permanent magnet (PM) incorporated in it. The structure is studied theoretically through flux linkage analysis, torque production, and magnetic circuit model (MCM) analysis. Next, the finite element technique (FEM) is used to model the suggested motor and the salient pole stator, both of which have the same size. Next, a comparison is made between the simulation findings and the static torque, PM demagnetization, flux linkage, magnetic flux density distribution, and average and maximum torque. The proposed design results in a 79.97% increase in average torque, a 90.89% increase in maximum torque, and a 3.02% decrease in cogging torque.

1. INTRODUCTION

Permanent magnet (PM) motors have several advantages, including high power, torque density, high efficiency, limited maintenance, and high dependability. These attributes make PM motors a good fit for application in a variety of industries, including electric vehicle (EV) [1, 2]. The fast advancement of PM materials in recent decades has made it possible to create high-performance permanent magnet synchronous motors (PMSMs) [3].

Based on where the magnet is positioned, PMSM is divided into two groups: interior (IPMSM) and surface (SPMSM) [4]. IPMSM is usually used in scenarios where there is a wide speed range, and SPMSM is often used in applications where the speed is constant. This is because it integrates the field weakening current and produces reluctance torque [5, 6]. Comparing an IPMSM motor to an SPMSM motor, the torque performance, power density, speed regulation performance, and cost of the former are better [7].

Additionally, an inner or outer rotor is used to run a PMSM. Because it guarantees that the air gap flux density amplitude roughly matches the PM's magnetic flux density, the inner rotor topology is used more frequently. This makes it possible to run a wider range of speeds and, in the end, results in a suitable capability to weaken the flux [8]. Also to note that the outer rotor has a nett mass that is 15% less than the inner rotor's, which reduces transmission losses [9].

* Corresponding authors: Hairul Faizi Hairulnizam (GS67769@student.upm.edu.my); Norhisam Misron (norhisam@upm.edu.my).

Although the outer rotor PM machine may produce a high torque density, a substantial amount of rare-earth PM material is needed [10]. The advancement of PMSM development is severely constrained by the rising cost of rare Earth PM, which raises PMSM manufacturing costs [11]. Considering this, the study mentioned in [12] looked at a variety of magnetic materials to investigate practical approaches for reducing or cutting the need for rare earth in PM motors. Findings from the study show that, despite being a rare-earth magnet, samarium performs the best at lower speeds, reaching an efficiency of 92.5% when running at full load. AlNiCo, on the other hand, has the best full-load efficiency, coming in at an astounding 75.7%.

In addition, to increase the performance of the motor, scientists also give top priority to improving the PMSM's structure, which includes the PM itself and the iron parts like the rotor and stator. The consequent-pole (CP) PM rotor is a technique that researchers have created to reduce dependency on PM rotors. Costs are greatly reduced by using this structure, which reduces PM volume by 30% [13–15]. Although the use of low-cost PM materials, such as ferrite, is an effective way to cut costs, insufficient torque density makes it difficult [16]. Based on its excellent performance features, like its high beginning torque and small number of permanent magnets needed, the results show that the V+1 type of PM structure is the best option.

Additionally, segmented (modular) construction has been used in PMSM because of its low production costs, high flexibility, and reduced windings [18–20]. A comparison of flux

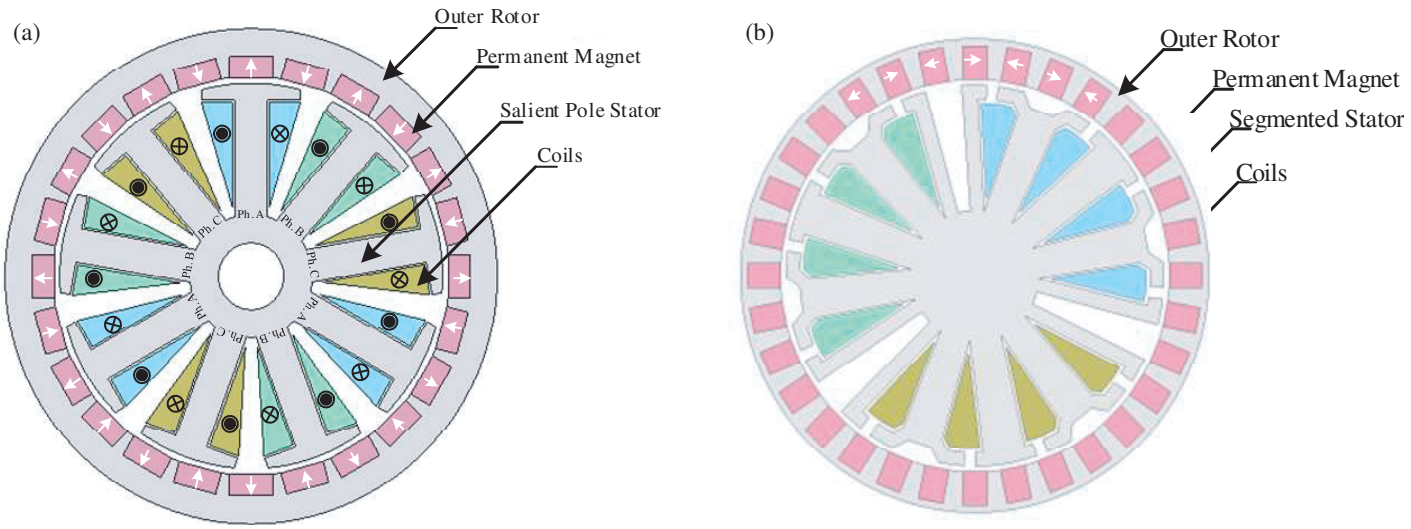

FIGURE 1. Structure of the (a) salient pole stator, (b) proposed segmented stator.

concentrating PM machines is shown in [21], where it is found that modular devices are more efficient than non-modular machines. Segmented structures, like divided teeth, have been widely adopted in switched reluctance motors (SRM) because they achieve a 93.3% higher efficiency compared to similar motors and significantly increase output torque by 63.91%, average torque by up to 60%, and both [22–24]. Adopting and combining the PM advantages of the PMSM with capabilities of the split teeth in the rotor and the segmented structure in the stator of SRM greatly improves the performance of the motor. This method lowers the quantity of PM used in the production of the motor.

This research aims to improve the salient pole stator by introducing a novel segmented stator structure that works in tandem with an embedded permanent magnet synchronous motor that has divided teeth on the outer rotor. The topology configuration and theoretical analysis that proved the superiority of the proposed motor are presented in Section 2. An equivalent salient pole motor and the suggested motor are simulated in two dimensions using finite element method. To verify the improved performance of the suggested structures, Section 3 compares the simulation results of the suggested motor with the salient pole stator of equal size in terms of flux linkage, magnetic flux density distribution, static torque, and dynamic torque. Section 4 illustrates the experimental and dynamic result in terms of torque speed characteristics. A conclusion is given in Section 5.

2. STRUCTURE AND THEORETICAL ANALYSIS

2.1. Structural Configurations

The salient pole stator PMSM's topology is shown in Figure 1(a). There are three phases in this motor, and each phase has three focused star connection windings. Its outer rotor features split teeth and embedded PMs. The PMs are positioned in the region between the rotor poles, which is magnetized in both the upward (N) and downward (S) directions, in contrast to the nearby magnets. A thorough assessment of the effects of a segmented stator on the suggested motor attributes, specifically about torque and power, are conducted using the nine branches of the salient pole stator, which is another feature of the salient pole stator.

The design of the suggested improved divided teeth outer rotor integrated permanent magnet with segmented stator, on the other hand, is shown in Figure 1(b). There are thirty-two poles on the motor's outer rotor. The PMs are positioned in the voids created by the rotor teeth. The magnetization direction of each new PM is facing and in opposition to the earlier one. By raising the magnetic flux density in the air gap, PMs are intended to increase torque and power densities. There are two focused windings in each of the motor's three phases. Additionally, there is a half pitch of magnet separation between each phase and four slots for each phase in the proposed segmented stator.

The stator structure is the main difference between the suggested motor's design and that of its equivalent. The equivalent uses a salient pole stator, while the proposed PMSM has a segmented stator. Furthermore, differences in the number and size of magnets may also influence the flux flow and flux density of the motor. It should be mentioned that the two motors' magnetization directions are different, which potentially affects how well the motor performs. The two motors differ in the number of connections in a phase and winding count, which may influence the flux flow within the motor. The key parameters and dimensions of the proposed motor are listed in Table 1.

2.2. Magnetic Flux Analysis

The flux flow of the salient pole stator is shown in Figure 2(a). When the coil is the only one energized, the flux flow is the same as in the proposed motor because the energized coil's magnetic field passes through air gaps, passes through the rotor and stator yokes, and ends at the excited phase windings of the pole. Due to the motor's alternating uphill and downward magnet arrangement, the flux flow in the open circuit intersected the air gaps at the stator pole and closed the flux loop at the

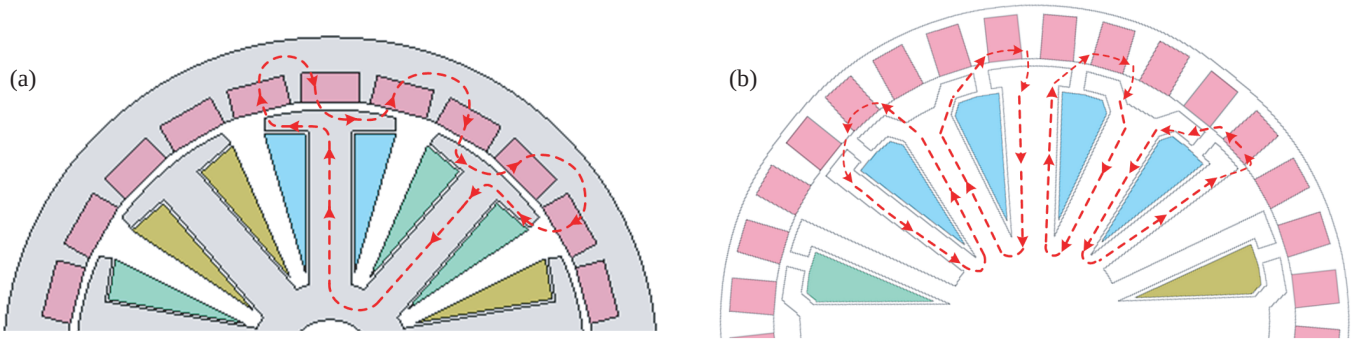

FIGURE 2. Predicted flux flow, (a) salient pole stator, (b) proposed segmented stator.

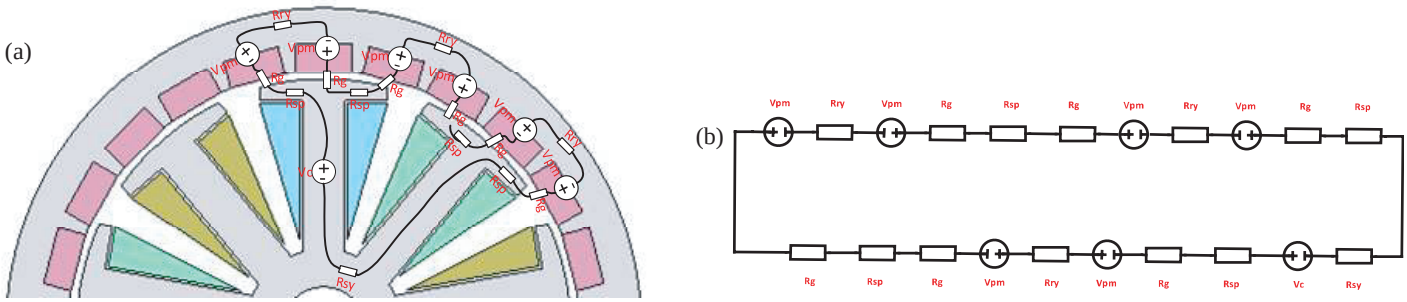

FIGURE 3. Salient pole stator, (a) magnetic circuit model, (b) simplified circuit.

TABLE 1. Key dimensions and parameter of the proposed motor.

Parameters	Salient pole stator	Proposed segmented stator
Number of phases	3	3
Stator outer radius (mm)	17.5	18.18
Rotor outer radius (mm)	22.5	22.5
Rotor inner radius (mm)	18	18.68
Number of turns per pole	10	13
Air-gap length (mm)	0.5	0.5
PMs width/length (mm)	2.0/4.0	2.38/3.18
Stack length (mm)	30	30
Number of magnets	24	32
Magnet material	NdFeB	NdFeB
Stator and rotor material	50H800	50H800

rotor yoke. The flux flows via the stator yoke, rotor yoke, and magnet when the winding is energized, closing the route at the neighbouring stator pole.

Figure 2(b) shows the projected flux lines to show how the suggested motor runs. When the coil is the only one that energizes, the magnetic field created by the coil passes through the air gaps, passes through the yokes of the stator and rotor, and ends at the excited phase windings of the pole. On the other hand, when the windings are open circuits, no current passes through them. The magnetic flux from the permanent magnet flows into the gaps between the rotor and stator when the armature winding is energized due to the force of the magnetic field. Every phase of the stator experiences flux flow via the central pole due to the growing magnetic flux in the air gaps. The flux flow in the motor is shortened when it is made to pass via the central stator pole. The motor's losses are decreased by a shorter flux flow. Consequently, a major factor in raising the air gap flux density in the suggested motor is the permanent magnets built inside the rotor. Figures 2(a) and (b) show the flux flow between segmented and salient pole motors, which have an impact on the motor's simulation performance.

2.3. Magnetic Circuit Model Analysis

The magnetic circuit model (MCM) for the salient pole and suggested motor is represented by Figures 3 and 4. Additionally, it encompasses the simplified circuit for the MCM. According to Figure 3, when Kirchhoff's Law is implemented, it may be said in terms of magnetic flux as an equation. In Equation (1), the its value is inadequate, in which $R_g \gg R_{sy} + R_{sp} + R_{ry}$

$$\Phi_{Salient\ Pole} = \frac{NI}{R_{sy} + 4R_{sp} + 3R_{ry} + 6R_g} \approx \frac{NI}{6R_g} \quad (1)$$

Conversely, according to Figure 4, when the same method is applied, with neglecting the value of other reluctances besides reluctance in air gap the magnetic field is represented as Φ.

$$\Phi_{Segmented} = \frac{NI}{R_{sy} + 2R_{sp} + 2R_{rp} + 2R_g} \approx \frac{NI}{2R_g} \quad (2)$$

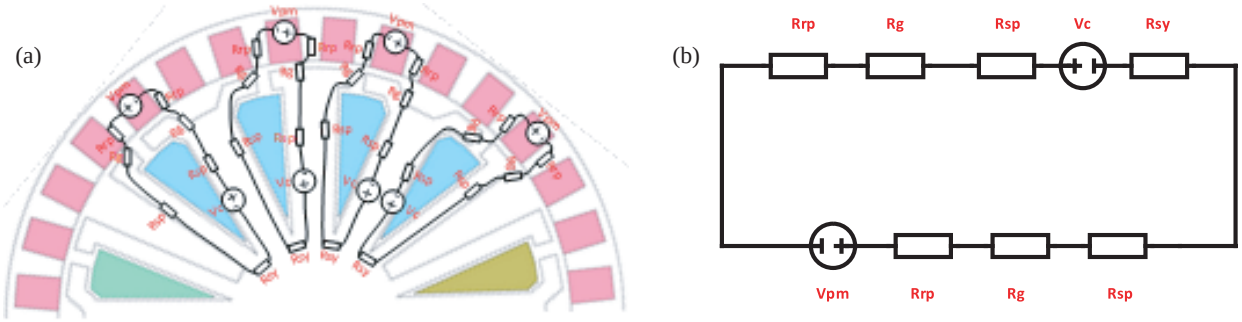

FIGURE 4. Proposed segmented stator, (a) magnetic circuit model, (b) simplified circuit.

Upon comparing Equations (1) and (2), the magnetic field generated in the proposed motor is greater than the salient pole, as shown in Equation (3). As there is a difference in magnetic field generated, it may influence the performance of motor.

$$\frac{NI}{6R_g} \ll \frac{NI}{2R_g} \tag{3}$$

where $\Phi_{Salient\ Pole}$ and $\Phi_{Segmented}$ are the magnetic flux for salient pole stator and magnetic flux for proposed segmented stator, respectively; N is the number of turns per phase; I is the current of each phase; R_g, R_{sy}, R_{sp}, R_{ry}, R_{rp} are the reluctance of air gap, stator yoke, stator pole, rotor yoke, and rotor pole, respectively.

2.4. Torque Generation Analysis

Due to their different topologies, the torques produced in segmented stator and salient pole configurations differ. The generic torque Equation (4) is then given to investigate the differences.

$$F = -\frac{\partial W}{\partial \theta} \tag{4}$$

where in general, energy (W) is stored in magnetic field, and θ is the position angle. Equation (5) shows the work done.

$$W = \frac{1}{2}\lambda i = \frac{1}{2}Ni\Phi = \frac{1}{2}Li^2 \tag{5}$$

W is also expressed in terms of flux linkage (λ), current (i), number of turns (N), magnetic flux (Φ), and inductance (L) expressed as Equation (6).

$$\Phi = \mathrm{N}iP = BA \tag{6}$$

P is represented as the permeance, which is the inverse of resistance (R). Hence, by using Equations (4), (5), and (6) the expression for thrust (F) may be derived as in Equation (7).

$$F = -\frac{1}{2}(Ni)^2\frac{\partial P}{\partial \theta} \tag{7}$$

The equation is further expanded as in Equation (8).

$$NI = N_cI_c + N_mI_m \tag{8}$$

The total magneto motive force (MMF), NI created in the motor is composed of the equivalent magnet MMF, N_mI_m produced in the rotor equipped with magnets, and the coil MMF, N_cI_c produced by the stator wound with the coil winding. When the values of N_cI_c and N_mI_m are evaluated, Equation (9) is derived.

$$\begin{aligned} F &= -\frac{1}{2}(N_cI_c + N_mI_m)^2\frac{\partial P}{\partial \theta} \\ F &= \frac{1}{2}(N_mI_m)^2\frac{\partial P}{\partial \theta} - (N_cI_c) \\ &\quad \cdot (N_mI_m)\frac{\partial P}{\partial \theta} - \frac{1}{2}(N_cI_c)^2\frac{\partial P}{\partial \theta} \end{aligned} \tag{9}$$

The cogging torque, which has the negative consequence of reducing the overall force produced by the motor, is the first term in the equation in Equation (9). The relationship between the coil flux and permanent magnet flux is represented by the second part of the equation. The final part of the equation computes the total force, which considers the contribution of the reluctance torque produced by the motor.

As per (9) which is obtained from a book in [25], the torque output of the comparison motor is done for cogging torque, the degree of interaction between coil flux and PM flux, and reluctance torque. The recommended motor is specifically designed to follow Equation (9), which seeks to maximize the interaction between coil flux and PM flux and minimize reluctance torque, while also minimizing cogging torque. With a little more work, the equation might be represented as in Equation (10), which is the fundamental formula for cogging torque, thrust, and reluctance torque, by replacing Equation (7) with Equation (9). All those components in the equation give required force F toward the capabilities of the motor.

$$F = \frac{B_g^2A}{2\mu_0} - NiBl - \frac{1}{2}\frac{\partial L}{\partial \theta}i^2 \tag{10}$$

2.5. Flux Linkage Analysis

Flux linkage, λ, refers to the connection between the magnetic field and the conductors of a coil. This occurs when the magnetic field Φ passes through the loops of the coil, which has N turns and expressed as in Equation (11).

$$\lambda = N\Phi \tag{11}$$

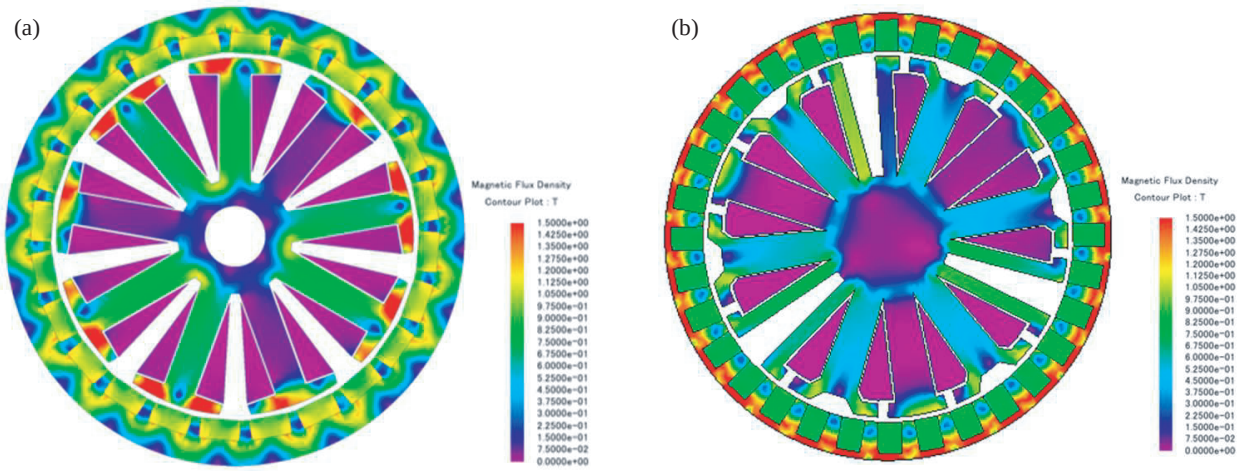

FIGURE 5. Magnetic Density of the (a) salient pole stator, (b) proposed segmented stator.

Here, the magnetic field, Φ, is deduced into Equation (12) as in Equation (12).

$$\Phi = \frac{LI}{N} \tag{12}$$

L is the inductance of the coil, while I stands for the current flowing through the stator. By adopting Equation (12) into (11), the flux linkage with the inclusion of inductance is defined as in Equation (13).

$$\lambda = LI \tag{13}$$

Furthermore, the total flux linkage in the energized phase (in this case phase A) is expressed as in Equation (14).

$$\lambda_{PA}=\lambda_i + \lambda_{PM} \tag{14}$$

where λ_{PA} represents the total flux linkage generated when phase A is excited; λ_i represents the flux linkage formed by the current flowing through the excited phase winding; and λ_{PM} represents the flux linkage made by the PM.

2.6. Finite Element Analysis

The application of Finite Element Analysis (FEA) is employed to find the fundamental magnetic properties of the motor under consideration. The electromagnetic characteristics of the suggested design are analyzed by simulating it using the 2-D finite element method (FEM). This research uses the JMAG software package developed by JSOL Corporation. The use of the two-dimensional finite element method (FEM) is favoured because of its rapid assessment through simulation and higher precision than the three-dimensional FEM. The electromagnetic characteristics of the motors are found using the Maxwell's equation, as depicted in Equation (15).

$$\begin{aligned}\Omega : \quad & \frac{\partial}{\partial x}\left(\upsilon\frac{\partial y}{\partial x}\right) + \frac{\partial}{\partial y}\left(\upsilon\frac{\partial y}{\partial y}\right) \\ = \; & -J - \upsilon\left(\frac{\partial Bry}{\partial x} - \frac{\partial Brx}{\partial y}\right) + \sigma\frac{\partial A}{\partial t}\end{aligned} \tag{15}$$

where Ω denotes the field solution zone of computation, A the magnetic vector potential, J the current density, υ the reluctivity, σ the electrical conductivity, and Bry and Brx represent as remanent flux density components.

Figures 5(a) and 5(b) show the magnetic density of the proposed segmented stator and the salient pole stator when the winding excited at 10 A. Both motors use the same material which is 50H800 steel for the rotor and stator. This material has a knee point saturation at 1.5 T. As seen, the stator of the proposed motor is not saturated which proves that the stator is well designed.

3. SIMULATION RESULTS

3.1. PM Demagnetization

The PM subjected to high currents may demagnetize in the suggested segmented stator. To verify that the PMs do not become demagnetized when being subjected to high current, a current of 5 A, or roughly 100% more than the rated current, is used to simulate both motors. The magnetic flux density distributions in the motor under a 5 A current are shown in Figure 7. NdFeB magnet, which has a 1.25 T saturation point, is used in both motors. The upper limit of the simulation is 1.25 T. Figure 6 makes it clear that, even at high currents, the recommended motor does not demagnetize the PM. But close to the knee point, the PM in the salient pole starts to saturate. The proposed segmented stator shows a notable advantage in this characteristic.

3.2. Flux Linkage

The flux linkage that happened in the two motors under study is as shown in Figure 7. The suggested motor produces a flux linkage from the magnets that is 79.86% bigger than its equivalent, as Figure 7(a) amply illustrates. The creation of electromagnetic torque in the motor is directly affected by the flux connection of permanent magnets. A mechanical torque is applied to the rotor because of the interaction between the coils carrying electric current and the magnetic field produced by the permanent magnets. The torque that the motor produces is what

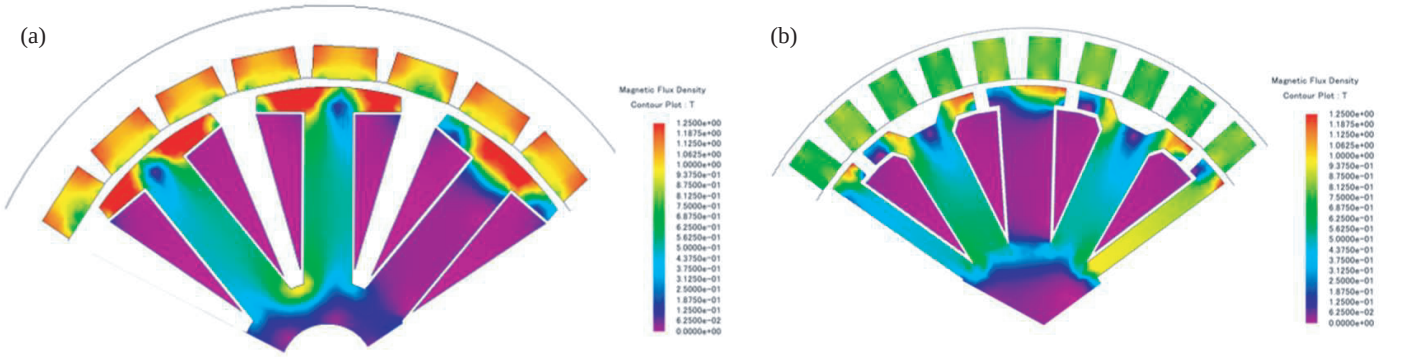

FIGURE 6. Magnetic flux density distribution of the magnet in (a) salient pole stator, (b) proposed segmented stator.

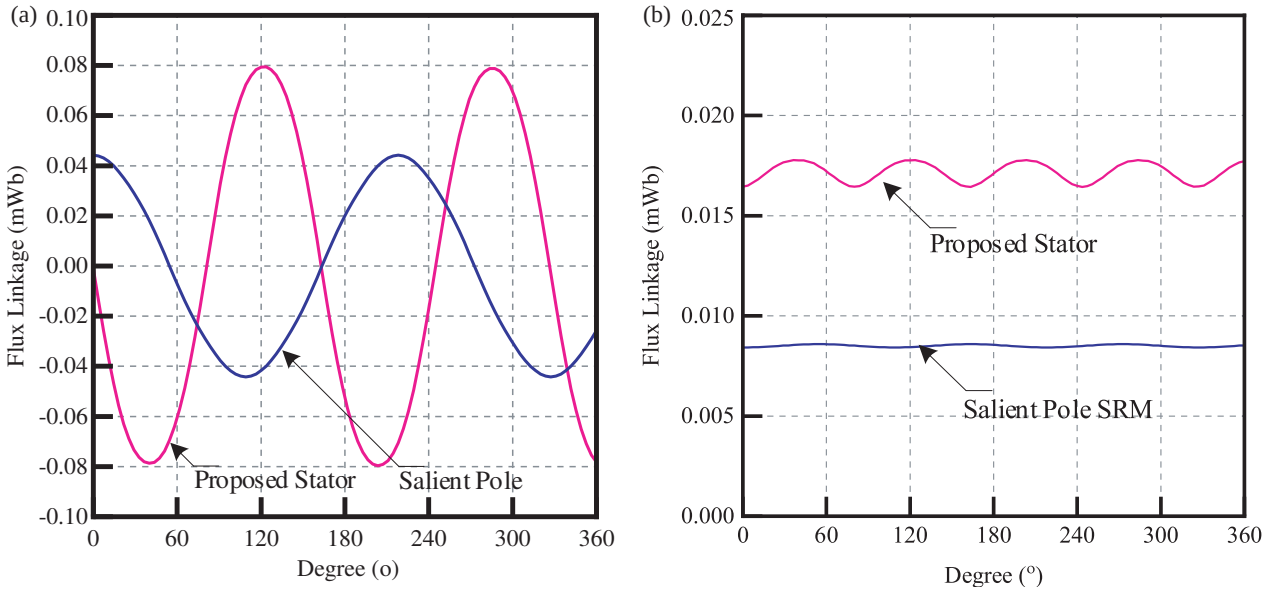

FIGURE 7. Flux linkage in both motor for (a) magnets, (b) coil inductance.

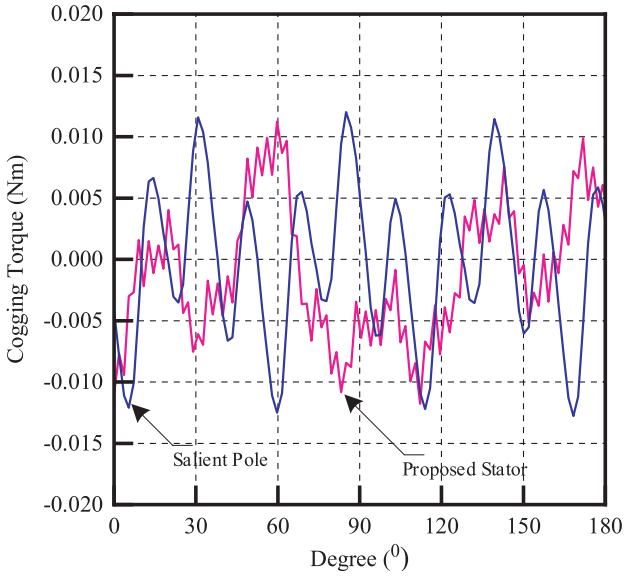

FIGURE 8. Cogging Torque profiles of the salient pole stator and proposed segmented stator.

drives its rotation and is directly correlated with the flux linkage of the permanent magnets. The coil inductance's flux linkage is depicted in Figure 7(b). The suggested motor has a ripple in its flux linkage, while the other motor has a value that is almost constant. It implies that the intended motor experienced the specified variations in inductance, as shown in Equation (9), to produce reluctance torque.

3.3. Analysis of Cogging Torque

Cogging torque is an undesirable property that negatively impacts a motor's performance. Reducing or eliminating the cogging torque is crucial for ensuring optimal motor performance. Cogging torque results from the interaction between the permanent magnet's magnetic flux lines and the stator's teeth. It occurs when there is no electrical current flowing through the coils, which prevents any of the coils from becoming energized. The permanent magnets in the system cause torque to exist even when there is no load.

The cogging torque of the conventional and proposed model is shown as in Figure 8. The highest cogging torque of the suggested motor is 0.01123 Nm, while the salient pole stator

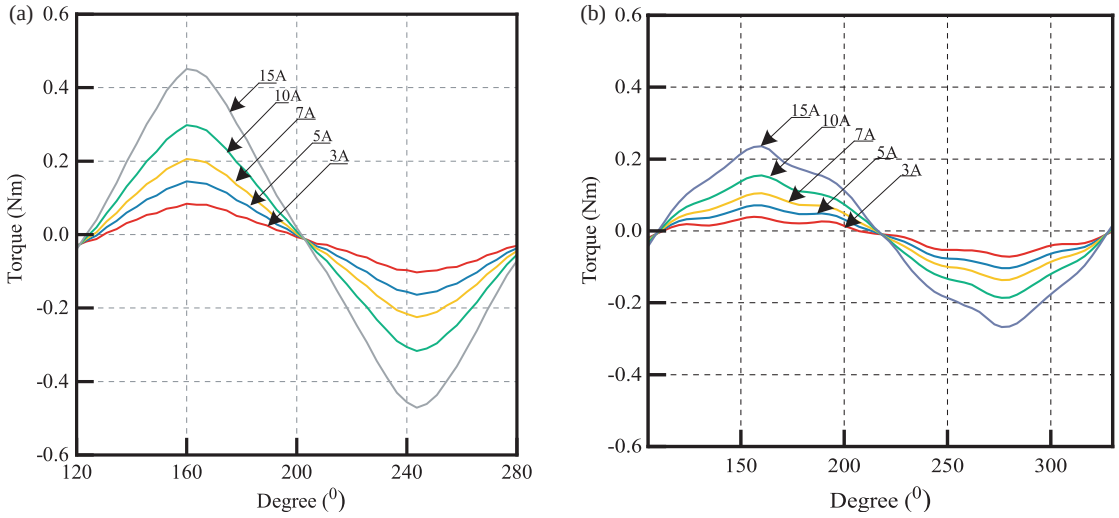

FIGURE 9. Static torque profile under different excitations current of 3 A, 5 A, 7 A, 10 A and 15 A for (a) proposed segmented stator, (b) salient pole stator.

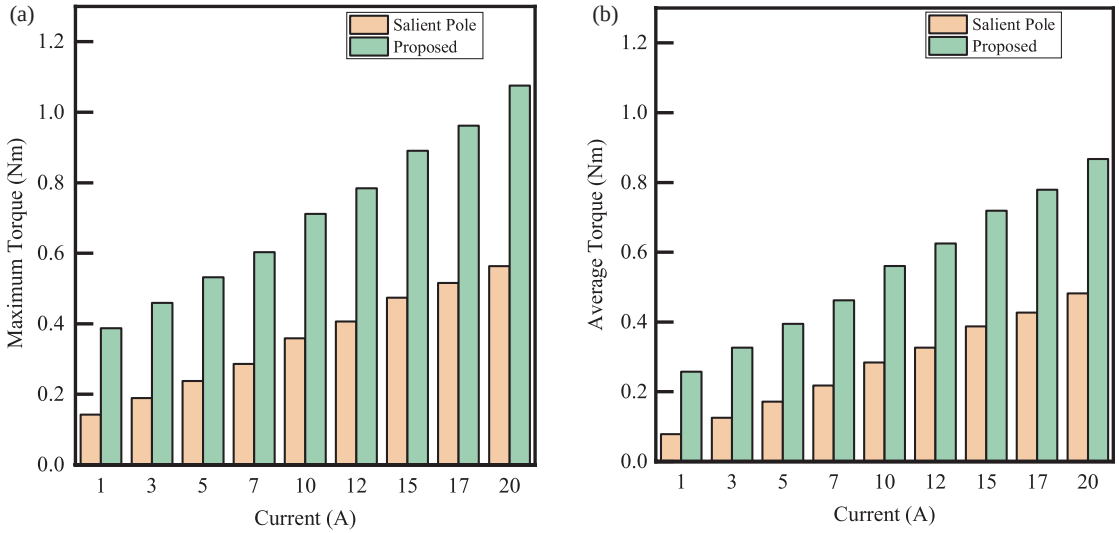

FIGURE 10. Comparison of (a) maximum torque, (b) average torque.

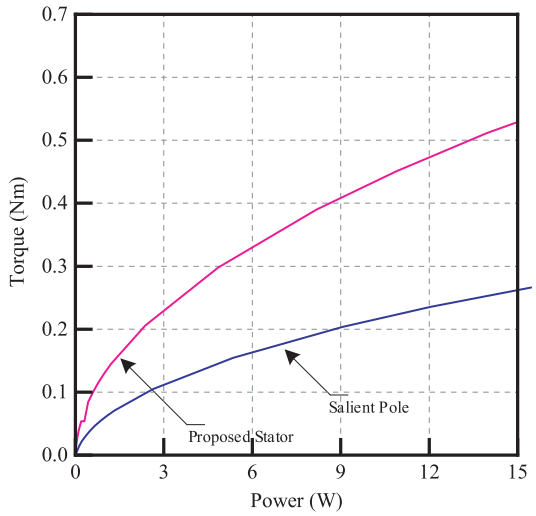

FIGURE 11. Power vs Torque.

motor's is 0.01158 Nm, 3.02% less than the equivalent version. Smaller cogging torque is produced at no-load performance because the permanent magnets' magnetic flux lines do not cross the air gaps. The careful placement of the PMs in both motor types is what yields the lowest cogging torque.

3.4. Analysis of Static Torque

Figures 9(a) and (b) illustrate the static torque profiles of the proposed motor and the salient pole stator, both of which are excited by a single-phase current. The torque profiles shown are in proportion to the rotor position at different excitation currents. The excitation modulates periodically at intervals of 3 A, 5 A, 7 A, 10 A, and 15 A. The graph proves a comparison of the overall static torque between the proposed motor and its counterpart, revealing that the suggested motor generates an 89.15% greater torque.

TABLE 2. Comparison of performance between the salient pole and the proposed stator.

Parameters	Salient pole stator	Proposed segmented stator	Differences (%)
Flux Linkage in Magnets (mWb)	0.044	0.079	79.86
Cogging Torque (Nm)	0.0115	0.0112	3.02
Static Torque at 15 A (Nm)	0.235	0.446	89.15
Maximum Torque at 20 A (Nm)	0.5632	1.075	90.89
Average Torque at 20 A (Nm)	0.4823	0.867	79.97
Torque when 9 W (Nm)	2.03	4.02	98.02
Stall Torque (Nm)	1.234	2.477	100.07
Torque at 3000 rpm (Nm)	0.246	0.439	78.45

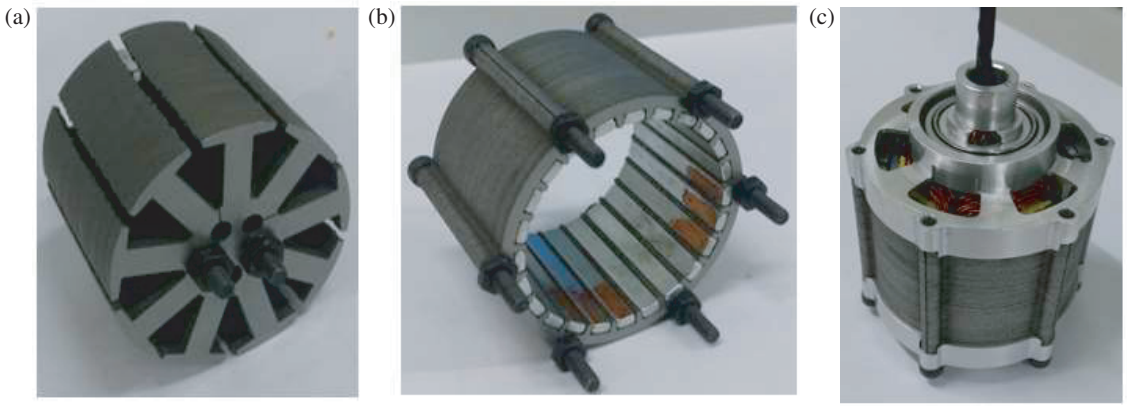

FIGURE 12. Fabricated component of (a) stator, (b) rotor and PM, (c) assembled motor.

To provide a more correct comparison, Figures 10(a) and (b) illustrate the maximum and average torque values within the 1–20 A range. The suggested motor shows superior maximum and average torque in all excitation currents compared to the counterpart motor. Additionally, the discrepancy in torque between the suggested and counterpart motors gets more pronounced with greater excitation currents. At a current of 20 A, the suggested motor showed a maximum torque of 90.89% higher and an average torque of 79.97% higher than the salient pole stator motor.

The relationship between power and torque is shown as in Figure 11. As the power increases, the torque of the suggested motor also increases. When the best power supply is decided to achieve the intended output torque, this graph may serve as a useful reference. Furthermore, it is observed that when an equal amount of power is supplied to both motors, the output torque produced by the suggested motor is greater than that of its counterpart. The disparity becomes increasingly pronounced as the power value rises. As an illustration, when running at a power of 9 W, the proposed motor surpasses its counterpart by 98.02% bigger output torque.

3.5. Comparative Analysis

Table 2 presents a comparative analysis of the performance of the salient pole stator and the proposed segmented stator. The table encompasses the parameters of the studies, the obtained results, and the percentages of differences that contribute to and illustrate the superiority of the proposed motor. The average torque increases by 79.97%; the maximum torque increases by 90.89%; and the cogging torque decreases by 3.02% because of the suggested design. These results demonstrate the superiority of the proposed segmented stator over the salient pole stator.

4. EXPERIMENTAL AND DYNAMIC RESULT

4.1. Fabrication and Experimental Setup

Figure 12(a) depicts the fabricated stator for the salient pole motor, whereas Figure 12(b) illustrates the fabricated rotor with embedded permanent magnets for the salient pole stator motor. The PM in the rotating iron is made of the material neodymium iron boron while the stator and rotor are made of 50H800 steel. The stator was wound with 1 mm diameter thickness coil with 10 turns as stated in Table 1. The motor has a stack length of 30 mm, and the air gaps that separated the stator and rotor were kept at 0.5 mm. Figure 12(c) depicts the constructed prototype of salient pole stator for testing. Figure 13 shows the experimental setup used to test the performance of the motor. The salient pole stator motor is tested with sensor less driver board to obtain the torque speed characteristic.

4.2. Torque Speed Characteristics

Figure 14 illustrates the torque-speed characteristics that are the focus of the dynamic result of the suggested motor in conjunc-

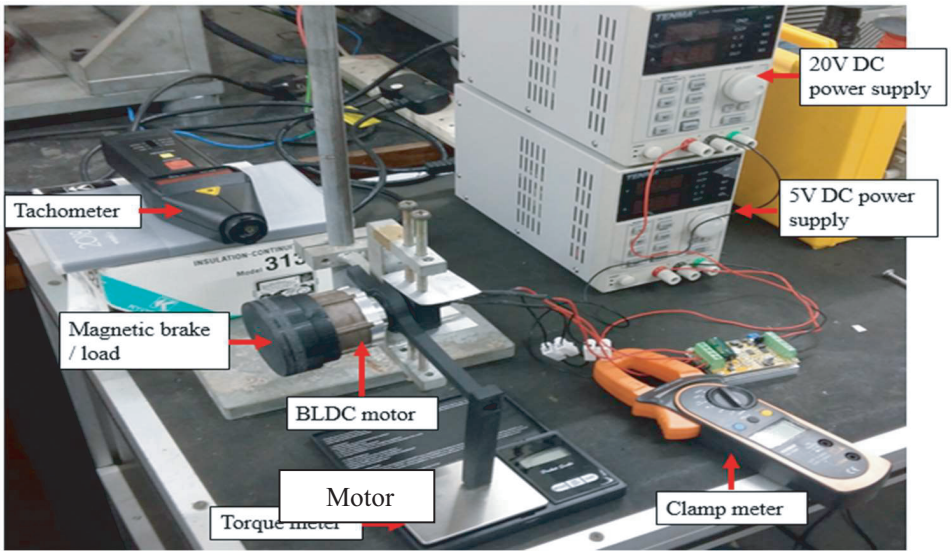

FIGURE 13. The testing setup for salient pole stator motor.

tion with the salient pole stator motor. The graph is plotted up to 5000 rpm, and the voltage injected into the motor is 20 V. This allows one to ascertain the motor's capability at both low and high speeds. It is evident that the suggested motor outperforms the salient pole stator in terms of stall torque, with a 100.07% increase. In terms of torque generation at the rated speed of 3000 rpm, the suggested motor performs better than its competitors, with an output torque that is 78.45% greater. Figure 12 also includes the salient pole fabricated result which is represented with solid symbols. As observed, the experimental and simulated results for the salient pole stator are similar and do not have much difference.

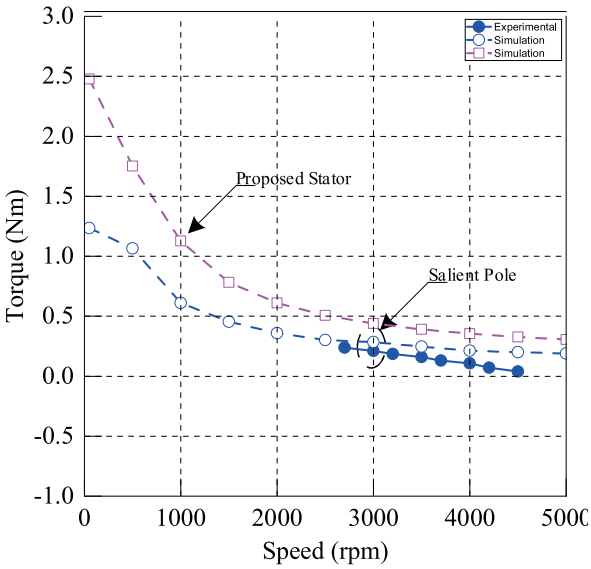

FIGURE 14. Torque speed characteristics of the simulated proposed segmented stator with the fabricated and simulated salient pole stator.

5. CONCLUSION

To enhance the salient pole stator PMSM, this work presents a new segmented stator structure with an integrated permanent magnet outer rotor. The first step is the design and operation of the suggested motor as well as its matching counterpart. To show the motor's remarkable torque capacity, MCM models of the motors were evaluated against the simulation design for its electromagnetic analysis. The results of the simulation showed that in terms of PM demagnetization, flux linkage, cogging torque, and static torques, the segmented stator architecture performed better than the other motor. The proposed design results in a 79.97% increase in average torque, a 90.89% increase in maximum torque, and a 3.02% decrease in cogging torque. These outcomes show that the suggested segmented stator is more efficient and better than the salient pole stator.

REFERENCES

[1] Liu, C., K. T. Chau, C. H. T. Lee, and Z. Song, "A critical review of advanced electric machines and control strategies for electric vehicles," *Proceedings of the IEEE*, Vol. 109, No. 6, 1004–1028, Jun. 2021.

[2] Wang, J., K. Atallah, Z.-Q. Zhu, and D. Howe, "Modular 3-phase permanent magnet brushless machines for in-wheel applications," in *2006 IEEE Vehicle Power and Propulsion Conference*, 1–6, Windsor, UK, 2006.

[3] Lee, C. H. T., W. Hua, T. Long, C. Jiang, and L. V. Iyer, "A critical review of emerging technologies for electric and hybrid vehicles," *IEEE Open Journal of Vehicular Technology*, Vol. 2, 471–485, 2021.

[4] Akatsu, K., K. Narita, Y. Sakashita, and T. Yamada, "Characteristics comparison between SPMSM and IPMSM under high flux density condition by both experimental and analysis results," in *2008 International Conference on Electrical Machines and Systems*, 2848–2853, Wuhan, China, 2008.

[5] Zhu, Z. Q., Z. P. Xia, Y. F. Shi, D. Howe, A. Pride, and X. J. Chen, "Performance of halbach magnetized brushless AC mo-

tors," *IEEE Transactions on Magnetics*, Vol. 39, No. 5, 2992–2994, 2003.

[6] Jahns, T. M., G. B. Kliman, and T. W. Neumann, "Interior permanent-magnet synchronous motors for adjustable-speed drives," *IEEE Transactions on Industry Applications*, No. 4, 738–747, 1986.

[7] Dong, J., Y. Huang, L. Jin, and H. Lin, "Comparative study of surface-mounted and interior permanent-magnet motors for high-speed applications," *IEEE Transactions on Applied Superconductivity*, Vol. 26, No. 4, 1–4, Jun. 2016.

[8] Vlachou, V. I., G. K. Sakkas, F. P. Xintaropoulos, M. S. C. Pechlivanidou, T. D. Kefalas, M. A. Tsili, and A. G. Kladas, "Overview on permanent magnet motor trends and developments," *Energies*, Vol. 17, No. 2, 538, Jan. 2024.

[9] Beniakar, M. E., P. E. Kakosimos, C. T. Krasopoulos, A. G. Sarigiannidis, and A. G. Kladas, "Comparison of in-wheel permanent magnet motors for electric traction," in *2014 International Conference on Electrical Machines (ICEM)*, 2472–2478, Berlin, Germany, 2014.

[10] Li, F., K. Wang, J. Li, and H. Y. Sun, "Electromagnetic performance analysis of consequent-pole PM machine with asymmetric magnetic pole," *IEEE Transactions on Magnetics*, Vol. 55, No. 6, 1–5, Jun. 2019.

[11] Guo, L., Q. Li, and H. Wang, "Design and analysis of consequent pole permanent magnet synchronous motor with low torque ripple," *IET Electric Power Applications*, Vol. 17, No. 4, 547–561, Apr. 2023.

[12] Romero, M. E., "Analysis and comparison of the interior permanent magnet motor design with different magnetic materials," in *2020 IEEE International Conference on Electro Information Technology (EIT)*, 249–254, Chicago, IL, USA, Sep. 2020.

[13] Chung, S.-U., J.-M. Kim, D.-H. Koo, B.-C. Woo, D.-K. Hong, and J.-Y. Lee, "Fractional slot concentrated winding permanent magnet synchronous machine with consequent pole rotor for low speed direct drive," *IEEE Transactions on Magnetics*, Vol. 48, No. 11, 2965–2968, 2012.

[14] Chung, S.-U., J.-W. Kim, Y.-D. Chun, B.-C. Woo, and D.-K. Hong, "Fractional slot concentrated winding pmsm with consequent pole rotor for a low-speed direct drive: Reduction of rare earth permanent magnet," *IEEE Transactions on Energy Conversion*, Vol. 30, No. 1, 103–109, 2015.

[15] Chung, S.-U., S.-H. Moon, D.-J. Kim, and J.-M. Kim, "Development of a 20-pole–24-slot SPMSM with consequent pole rotor for in-wheel direct drive," *IEEE Transactions on Industrial Electronics*, Vol. 63, No. 1, 302–309, Jan. 2016.

[16] Petrov, I. and J. Pyrhonen, "Performance of low-cost permanent magnet material in PM synchronous machines," *IEEE Transactions on Industrial Electronics*, Vol. 60, No. 6, 2131–2138, 2013.

[17] Wang, M. and Z. Chen, "Research on permanent magnet structure of permanent magnet synchronous motor for electric vehicle," in *2022 2nd International Conference on Electrical Engineering and Control Science (IC2ECS)*, 990–993, Nanjing, China, 2022.

[18] Lin, C.-C. and Y.-Y. Tzou, "An innovative multiphase PWM control strategy for a PMSM with segmented stator windings," in *2015 IEEE Applied Power Electronics Conference and Exposition (APEC)*, 270–275, Charlotte, NC, USA, 2015.

[19] Aggarwal, A., E. G. Strangas, and A. Karlis, "Review of segmented stator and rotor designs for AC electric machines," in *2020 International Conference on Electrical Machines (ICEM)*, Vol. 1, 2342–2348, Gothenburg, Sweden, 2020.

[20] Li, G.-J., Z.-Q. Zhu, M. P. Foster, D. A. Stone, and H.-L. Zhan, "Modular permanent-magnet machines with alternate teeth having tooth tips," *IEEE Transactions on Industrial Electronics*, Vol. 62, No. 10, 6120–6130, Oct. 2015.

[21] Spooner, E. and A. Williamson, "Modular, permanent-magnet wind-turbine generators," in *IAS '96. Conference Record of the 1996 IEEE Industry Applications Conference Thirty-First IAS Annual Meeting*, Vol. 1, 497–502, San Diego, CA, USA, 1996.

[22] Kumawat, S., S. Bhaktha, and K. V. Gangadharan, "Enhancing torque performance with dual teeth switched reluctance motor: A novel approach," in *2021 IEEE International Power and Renewable Energy Conference (IPRECON)*, 1–6, Kollam, India, 2021.

[23] Farahani, E. F., M. A. J. Kondelaji, and M. Mirsalim, "Divided teeth switched reluctance motor with different tooth combinations," in *2020 11th Power Electronics, Drive Systems, and Technologies Conference (PEDSTC)*, 1–5, Tehran, Iran, 2020.

[24] Liu, C., K. T. Chau, C. H. T. Lee, F. Lin, F. Li, and T. W. Ching, "Magnetic vibration analysis of a new DC-excited multitoothed switched reluctance machine," *IEEE Transactions on Magnetics*, Vol. 50, No. 11, 1–4, Nov. 2014.

[25] Oshinoya, Y., *Electrical Machine*, 2005.